Interactions between Global Change and Human Health
Pontifical Academy of Sciences, *Scripta Varia* 106, Vatican City 2006
www.pas.va/content/dam/accademia/pdf/sv106/sv106-ruddiman.pdf

PRE-INDUSTRIAL DEPOPULATION, ATMOSPHERIC CARBON DIOXIDE, AND GLOBAL CLIMATE

WILLIAM F. RUDDIMAN[1] & ANN G. CARMICHAEL[2]

The topic addressed by this volume – interactions among human health, global change, and socio-economic factors – is immensely broad and complex. In this paper, we focus on one of many related issues – the link between population size (one of many possible indices of human well-being), atmospheric carbon dioxide (CO_2), and climate during the pre-industrial portion of the historical interval. Specifically, we test a new hypothesis that intervals of significant human depopulation (at the scale of tens of millions of deaths) caused reforestation of abandoned farmland, and thereby reduced atmospheric CO_2 concentrations and cooled global climate.

In the first section of this paper, we focus on the major multi-regional depopulation intervals identified in historical records. We summarize the likely impacts of famine, war, and disease on depopulation and conclude that disease is the largest factor in most major depopulation intervals. We conclude that the correlation between major pandemics and intervals of decreased CO_2 supports a causal link between mass mortality and carbon levels in the atmosphere. In the second section, we outline the methods used to analyze and quantify possible pandemic-climate links. In the third section, we model the response of atmospheric CO_2 concentrations to carbon input and removal caused by reforestation, by decreases in rates of deforestation, and by decreases in early coal use. We find that reforestation was probably the major contributor to CO_2 decreases during depopulation intervals, while reductions in rates of deforestation and coal use were likely secondary factors.

[1] Department of Environmental Sciences, University of Virginia, Charlottesville, VA.
[2] Departments of History and HPSc, Indiana University, Bloomington, IN.

1. Links Between Depopulation, Disease, and Climate

All dates cited in this paper are in years CE (current era), unless otherwise specified.

1.1. *Pandemics and Depopulation*

Historical changes in human populations for Europe, China, and the Americas, as well as all other regions combined, are shown in Figure 1. Three areas – Europe, China, and the Americas – were plotted individually because they show major depopulation during several pre-industrial intervals. For most of Eurasia, these population data are from McEvedy and Jones (1978), who noted that their estimates varied by ±20% relative to other compilations based on similar sources. More recent estimates of Chinese population from Lee and Feng (1999) were used, even though in most cases continental scale estimates differ little from those in McEvedy and Jones for the period before the late 1600s. Early population estimates for several countries that are lumped together as 'other' in Figure 1 are poorly constrained: India prior to the Mughal era (1500s), and Indo-China, sub-Saharan Africa and Oceania even in later centuries.

Population estimates for the Americas are taken from Denevan (1992), who proposed an indigenous population of 55 million on the eve of European contact, followed by a precipitous drop over the next two centuries to 5 or 6 million. Formerly, such calculations depended on backward projections from Spanish and Portuguese censuses of native populations and on mortality rates extrapolated from local examples. More recently, new forms of archeological study such as air-photo and remote-sensing surveys of ancient structures built for agriculture and transportation have provided additional support for higher population estimates. The backward projection of the American population shown in Figure 1 prior to European contact is based on a 1500-year doubling time for population growth. We make no attempt to address regional fluctuations in population in the Americas before contact with Europeans, such as the collapse of Mayan civilization in the 800s and 900s or the smaller-scale contraction and displacement of the Anasazi in the 1300s.

The generally exponential rise of populations through historical time reflects a host of factors that affected people and their food supplies. Innovations in agricultural methods and technology, introduction of non-indigenous foods (plant and animal), and social policies all played a role.

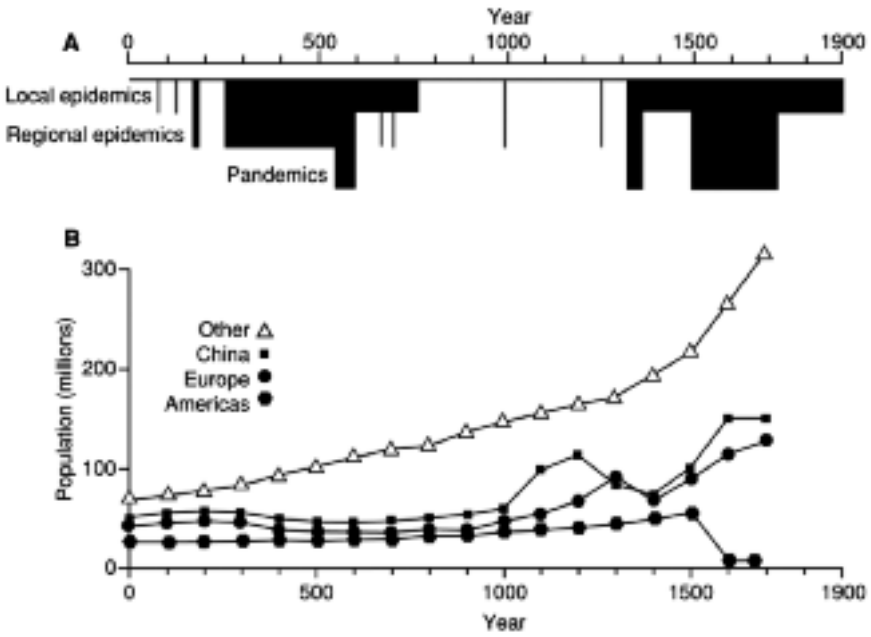

Figure 1. Link between pandemics (A) and major depopulation episodes (B) during the last two millennia. Major population drops in Europe and China from McEvedy and Jones (1978) and in the Americas from Denevan (1992).

Despite general population growth, every pre-industrial civilization also experienced intervals of stagnation or depopulation (Landers, 2004). The classical Malthusian checks of famine and disease, enhanced by warfare, are frequently assumed to have driven periods of stagnation and decline. Chinese populations uniquely limited fertility through infanticide (Lee and Feng, 1999; Lavely and Wong, 1998).

Among the intervals of decline lasting a century or more, we can distinguish in the sketchy historical records before 1800 a few dramatic episodes of population loss that were concentrated within a decade. Here we first explore the possible causes of these major depopulation episodes – famine, warfare, or acute exogenous epidemic disease.

The hypothesis that famine accounts for intervals of large-scale depopulation has largely been rejected. Even the worst famine of the last millennium in Western Europe, from 1315 to 1322, claimed no more than 10% of the population in northwestern Europe, where its effects were

strongest (Jordan, 1996; Watkins and Menken, 1985, 1988). Where not complicated by warfare or the loss of livestock to pestilence, population numbers rebounded before the catastrophic Black Death a few decades later. Population recovery occurred rapidly because famine and the additional diseases it causes primarily take the lives of the very young and the 'elderly' (at that time, those over 45 years of age). Large famines did not recur in pre-industrial European populations; only the difficult years from 1815-1818 compare in geographical extent with the 1315-1322 period. Although significant short-term famine mortality also occurred elsewhere, including large areas of China during the early 1580s and 1640s (Dunstan, 1975), the Chinese imperial state early initiated interregional transfers of food to avert famine (Marks, 1998; Shiue, 2005). By the late eighteenth century, famine crises in Europe, North Africa, and Asia had also been largely solved by regional transportation of grain and by credit financing that gave the affected populations and governments purchasing power in larger markets (Ó Gráda, 2005).

War is also not a first-order factor in most of the intervals of major depopulation, although two periods of intensive warfare merit comment. During the Thirty Years' War in Europe (1618-1648), mortality was abnormally high because civilians were frequently targets of military actions. An estimated 8 million people died in German regions and in Belgium (Gutmann, 1980), but even that number did not reach the levels during the major depopulation intervals plotted in Figure 1b. War and political upheaval, however, did precipitate major depopulation during at least one interval in Chinese history. From 1278 to 1369, the occupying Mongol rulers of northern China (the Yuan dynasty) destroyed much of the ecological and economic infrastructure, leading to catastrophic population losses in the north, as well as localized epidemics and famines. In this case, 25 to 50 million people are thought to have died. Millions likely fled south, to the southern Song dynastic region, with some estimates of regional depopulation in the once prosperous north as high as 86% (Deng, 2003).

With the exception of China, disease is the primary explanation of the great depopulation episodes of human history. Infectious and non-infectious diseases regularly pruned pre-industrial populations before the sanitary revolution of the late nineteenth century, but they did not for the most part result in major fluctuations over decades or centuries (Bourdelais, 2003; Livi-Bacci, 2001). This pruning can be regarded as a 'steady-state' phenomenon: always in action, always culling a share, but not causing discrete population drops.

In contrast, a few acute infectious diseases – principally plague in Europe and various viral rashes in the Americas – were 'pandemic' agents that led to a few great depopulation episodes. Demographically, bubonic plague affects at-risk populations indiscriminately with respect to age and gender. Plagues killed people during their reproductive years and were accompanied or followed by non-plague epidemics; the combination had a lasting negative effect on population recovery (Hatcher, 1977; Paine, 2000). Smallpox and measles introduced in the Americas had similarly extensive, multi-regional effects. Temporally these epidemics lasted a century or more, and the losses were much higher than those caused by other diseases. The impacts of three major pandemics are obvious in the population trends in Figure 1.

The first major interval of large-scale depopulation in Mediterranean and Western Europe began with the so-called Antonine plague of 165-180. Although the principal microbial cause of this epidemic is debated, population loss was geographically and demographically extensive within the Roman Empire, including populous North Africa (Duncan-Jones, 1996; Scheidel, 2001). During the centuries after 200, McEvedy and Jones (1978) estimate a cumulative population loss of 40% (~10 million people) in southern and western Europe, but lesser mortality in the more sparsely populated north and east. The interval between 200 and the early 500s was one of general depopulation, punctuated by brief periods of partial recovery. Other diseases may have been involved in these ongoing losses, as well as socio-economic factors. Sallares (2002) suggests that malaria had a substantial demographic impact on the later Roman Empire.

The 'Plague of Justinian' in 540-542 was far more severe and spread across the entire continent of Europe (Stathakopoulos, 2004). Narrative accounts of Justinian's plague suggest that bubonic plague, caused by *Yersinia pestis*, was the principal agent of recurrent epidemic crises (Sarris, 2002). Plague recurred repeatedly from the sixth to the eight centuries from the Mediterranean west to Ireland and east to the lands of Islam, and probably spread farther east along the Silk Road (Twitchett, 1979).

The 'Black Death' pandemic of 1347-1353 in Europe, the Middle East, and North Africa offers better evidence of abrupt and protracted population decline. In regions where depopulation ratios can be calculated, Black Death losses reached the 30 to 45% level (a total of 25 to 33 million people). Plague, most likely caused by *Yersinia pestis*, and other epidemic infectious diseases recurred frequently in Europe during the century following this catastrophe, and population stagnation persisted well into the

1400s (Hatcher, 1994). The region now comprising Poland, Lithuania, Latvia, and northern Russia initially remained relatively unscathed, but populations in these regions collapsed half a century later.

Regional as well as dramatic localized plagues persisted in Europe until the mid-seventeenth century, with a final epidemic in Marseilles and Languedoc in 1720-22. Specific urban plagues during the period 1550 to 1720 caused mortality rates as high as 25 to 40% in parts of southern and central Europe, the only region where plagues seemed to have caused overall declines in population after 1600. Parish registers in German-speaking regions show that smaller settlements suffered even greater depopulation than urban centers (Eckert, 1996).

Even the extraordinarily high losses from recurrent plague and pestilence in Europe and the lands of Islam were still less devastating than the effects of common 'old world' infections on the native populations of the Americas. In addition to the diseases to which European, Asian and African populations had partial immunity, Native Americans were subjected to a host of diseases introduced by European livestock. The result was unprecedented mortality – depopulation without even partial recovery. An estimated 80 to 90% of the pre-Columbian population (50 to 60 million people) died between 1500 and 1800, with the highest losses in heavily populated regions probably occurring in the 1500s and 1600s (Denevan, 1992; Richards, 2003).

The role of disease in depopulating China was less predominant than in the west (Elvin, 1993). Of the two periods of great epidemics mentioned in Chinese historical sources, that of 636-655 seems to correspond with the spread of plague eastward along the Silk Road (Twitchett, 1979). A second wave of epidemics spread through more than half of North China from 698 to 713, reaching Korea and possibly Japan. Outbreaks in the 730s are more securely identified as smallpox. In areas where the best records survive, Japan's registered population in 726 ranged from 23 to 90% below that of 609. Over the next millennium, until the 1600s, the worst losses occurred in areas of longstanding warfare. Dunstan (1975) and Chang (2002) show that the Manchu conquest of the late 1630s, displacing the Ming dynasty by 1644, was particularly troubled by smallpox epidemics. The extensive and widespread mortality among those being incorporated into this new regime prompted the first extensive treatise on large-scale epidemic diseases within traditional Chinese medicine.

The overall doubling of human global population from 400-500 million in 1500 to 850-950 million in 1800 owed much to improvements in

both regional and global transportation of food and to the availability of credit (Richards, 1997). Most of the population rise during the modern period in India and Japan (late sixteenth-seventeenth centuries) and in China and Europe (eighteenth century) occurred through consolidation and stability of political power. The Americas did not regain pre-Columbian population levels until the nineteenth century, and this only by virtue of European immigration and expansion.

1.2. *Linking Pre-Industrial Depopulation Intervals, CO_2, and Climate Change*

Recent advances in climate science have provided valuable new information on climate change during the historical era. The first proxy-based reconstruction of temperature spanning the last millennium at a hemispheric scale was that of Mann *et al*. (1999). This and subsequent efforts have been based on records in climatic archives such as ice cores, tree rings, and corals. Dozens of records have been analyzed to extract a common temperature signal weighted so as to avoid bias from the uneven spatial distribution of the records.

Several other reconstructions of northern hemisphere temperature changes during the last millennium show similar patterns but varying amplitudes (Crowley and Lowery, 2000; Jones *et al*., 2001; Jones and Mann, 2004). In higher (Arctic) latitudes, reconstructed temperature changes over decadal intervals are generally larger by a factor of 2 or 3 than hemispheric averages (Overpeck *et al*., 1997; Esper *et al*., 2002). This poleward amplification is consistent with the larger temperature variability observed today during cold seasons near sensitive snow and sea-ice boundaries. Moberg *et al*. (2005) recently reconstructed changes in temperature much larger than those in Mann *et al*. (1998) and Crowley and Lowery (2000). But the disproportionate number of proxies from polar latitudes used in the Moberg reconstruction may invalidate it as a representative hemispheric-mean signal.

The first attempt to extend the northern-hemisphere temperature reconstruction towards the start of the historical era in Europe is shown in Figure 2a (Mann and Jones, 2003). The shaded region indicates the large uncertainties resulting from the sparse coverage of sites and the imprecise links of the proxy indicators to temperature. A comparison of the trends in Figures 1b and 2a hints strongly at a correlation between cooler climates and intervals of major regional depopulation. Cooler temperatures prevailed during the slow European population decrease between 200 and 800,

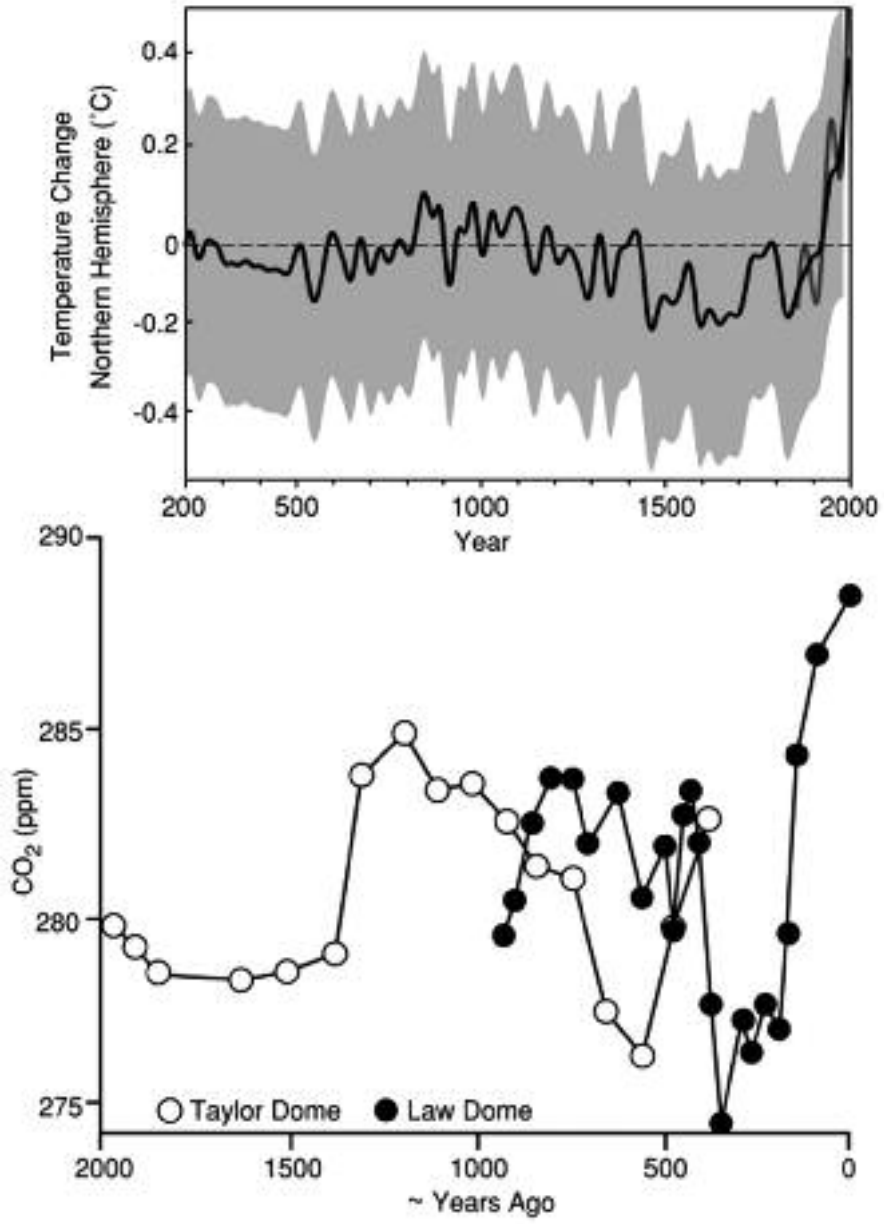

Figure 2. Reconstructed trends in northern hemisphere temperature (top) from Mann and Jones (2003) and atmospheric CO_2 concentrations (bottom) from Etheridge *et al*. (1996) and Indermuhle *et al*. (1999).

and again from 1500 to 1750, the time of the American pandemic. Warmer conditions prevailed during the intervening pandemic-free era.

Given this apparent link between intervals of major depopulation and large-scale climate change, an obvious question is what kind of mechanism might account for it. The greenhouse gas, carbon dioxide (CO_2), plays an important role in climate change, and its past concentrations in the atmosphere can be measured in air bubbles trapped in ice drilled in Antarctica. Plotted in Figure 2b are records of CO_2 concentrations from two sites. The record from Law Dome (Etheridge *et al*., 1996) is the better dated because it contains layers of volcanic ash particles from explosions of known age (Palmer *et al*. 2001). Dating of the record from Taylor Dome (Indermuhle *et al*., 1999) is far less secure: it is based on correlating the methane signal at Taylor Dome to that of an annually layered (and thus well dated) ice core from Greenland. Uncertainties for the Taylor Dome record derived in this way are estimated at ~500 years prior to 1000, and ~100 years during the most recent millennium.

The conventional interpretation of these historical CO_2 trends is that they are driven by natural variations in the frequency of volcanic explosions and by small changes in the radiative output of the Sun over decadal and century time scales (Crowley, 2000; Gerber *et al*., 2003). In this view, both the CO_2 oscillations and the temperature changes shown in Figure 2 are natural responses of the climate system to the same solar-volcanic forcing.

This explanation can be evaluated with carbon cycle models that quantify both the size of the CO_2 oscillations and the amount of global (or hemispheric) temperature change that would result from solar-volcanic changes (Gerber *et al*., 2003). The models indicate that solar-volcanic forcing sufficient to cause a CO_2 oscillation of 1 ppm (part per million) should produce a temperature response of 0.08°C. Gerber *et al*. (2003) compiled a composite CO_2 curve by stacking and averaging individual CO_2 records from four ice cores. Because several of the largest CO_2 oscillations are offset among individual cores (as in Figure 2b), this procedure yielded a smoothed record with maximum CO_2 variations of ~4 ppm. This value seemed roughly consistent with the CO_2 change that the model predicted should accompany the temperature variations in Figure 2.

Ruddiman (2003) viewed these CO_2 records in a different way. He noted that both ice-core records in Figure 2b have CO_2 oscillations as large as 8 ppm, as did an early record from Adelie Dome (Barnola *et al*., 1995). He thus proposed that the large CO_2 changes are real but that inadequate dating control caused these oscillations to be misaligned (offset in age) from record to record.

If the CO_2 drops really were as high as 8 ppm, the solar-volcanic explanation cannot account for them without violating the constraint imposed by the small changes in reconstructed temperature. For example, the average cooling between the intervals 900-1100 (the 'Medieval warm interval') and 1500-1800 (the 'Little Ice Age') is no more than 0.3°C (Figure 2a), consistent with a CO_2 drop of ~3.5 ppm. Yet the CO_2 drop between those two intervals in the well-dated Law Dome ice core is ~8 ppm (Figure 2b), leaving 4 to 5 ppm of the observed change to be explained by factors other than natural forcing.

Subsequent work has further highlighted the shortcomings of natural factors as an explanation of these CO_2 decreases. CO_2 changes in well-dated ice from Dronning Maud Land and South Pole confirm a CO_2 drop of at least 8 ppm from 1100 to 1700 (Siegenthaler *et al.*, 2005). Those authors also concluded that the Little Ice Age cooling, which is small in amplitude and centered in the North Atlantic region, is unlikely to explain so large a CO_2 drop. This apparent failure of the solar-volcanic explanation to account for the large observed changes in CO_2 invites a different explanation.

1.3. *The Pandemic-CO_2-Climate Hypothesis*

An alternative explanation for the large CO_2 oscillations-human activities arose as a corollary to a recent hypothesis. Ruddiman (2003) pointed out that the gradual rise in CO_2 and methane values during the last several millennia is anomalous compared to trends during similar intervals in the early portions of previous interglaciations (Figure 3, see page 410). Previously, CO_2 values rose to a strong peak just before the start of each interglaciation and then declined steadily through the next 10,000 to 15,000 years of each early-interglacial interval. Early in the present interglaciation, CO_2 reached a similar peak 10,500 years ago and began to decline as it had before. Beginning around 8000 years ago, however, a large CO_2 increase occurred that had no precedent in previous interglaciations.

Ruddiman (2003) proposed that humans were responsible for this anomalous CO_2 increase, primarily by clearing and burning forests in southern Eurasia to open land for farming. Carcallet *et al*. (2002) had independently inferred a possible human role in the CO_2 increase of the last 8000 years, based on increased deposition rates of charcoal on several continents. Ruddiman (2003) also suggested that major increases in rates of human mortality might be the explanation of the century-scale CO_2 oscillations near the end of the Holocene CO_2 rise. He proposed that pandemics –

outbreaks of bubonic plague and other diseases on a multi-continental scale – are the most plausible mechanism for linking changes in human populations, atmospheric CO_2, and global climate. The link proposed was large-scale reforestation of farms abandoned as a result of pandemics, and subsequent sequestration of atmospheric carbon in the growing forests.

The correlations among pandemics, depopulation episodes, decreases in CO_2, and cooler temperatures in Figures 1 and 2 support this explanation, particularly if allowance is made for the uncertainties inherent in historical estimates of human mortality, in dating the CO_2 signals, and in the pattern and amplitude of the temperature reconstruction. In addition, the evidence from China discussed earlier further indicates that at least one depopulation episode (during the Yuan dynasty, 1278-1369) could have resulted from conquest and social policy. The population losses in that episode also had the potential to affect the global carbon budget because prior to population collapse, northern China had turned to coal as a primary fuel source, having exhausted the accessible forest reserves (Hartwell, 1962, 1967).

If depopulation episodes contribute to changes in atmospheric CO_2 concentrations, it makes sense to ask whether or not the observed CO_2 changes could have driven the reconstructed changes in northern hemispheric temperature. Based on a widely used estimate of Earth's temperature sensitivity to CO_2 changes (IPCC, 2001), the CO_2 drop of 8 ppm between the maximum at 1100-1200 and the minimum at 1500-1800 should have caused global and hemispheric temperature to fall by ~0.1°C. Over this same interval, the average temperature decrease (using century-scale averages and ignoring decadal-scale variations) was 0.15-0.2°C (Fig. 2a). As a result, the observed CO_2 decrease appears to explain half or more of the drift toward colder temperatures from the warmer medieval era to the peak expression of the so-called little ice age (1550 to 1800).

In summary, the model simulation of Gerber *et al*. (2003) indicates that natural forcing cannot explain a CO_2 drop of 8 ppm during the last millennium without violating the small temperature cooling reconstructed for the northern hemisphere. A factor new to the 'natural' workings of the climate system – human history – appears to have played a significant role in both the CO_2 and temperature changes of recent millennia. This hypothesis immediately raises the question of whether human populations really were large enough centuries or millennia ago to have had an impact on atmospheric CO_2 concentrations. The purpose of the rest of this paper is to make a quantitative assessment of this idea.

1.4. *CO_2 Target Signal for Testing the Pandemic-CO_2-Climate Hypothesis*

The CO_2 trends at Taylor and Law Domes from Figure 2b are combined into a composite target signal in Figure 4 (see page 410). The well-dated Law Dome record subsequent to 1100 years ago serves as the target signal. Prior to that time, we are forced to rely on the less securely dated record from Taylor Dome. The intervals of large-scale depopulation discussed earlier correspond to three periods of CO_2 decreases in Figure 3: (1) a small but long-lasting drop of ~2 ppm during the epidemics and pandemics of the late Roman Era between 200 and 600 AD; (2) a short ~2 ppm decrease during the Black Death (bubonic plague) pandemic of 1350 and subsequent outbreaks in the next century; and (3) an abrupt drop of ~5 ppm soon after the start of the American pandemic era in the 1500s.

For the analysis that follows, we need to consider how faithfully the ice cores might record very rapid changes in atmospheric CO_2. The initial Black Death pandemic (1347-1353) represents the most extreme case: large changes in population occurred within a few years, and resulting changes in carbon emissions and sequestration within a few decades. In contrast, the large changes between 200 and 600 and between 1500 and 1750 occurred over centuries.

Because of exchanges of air in the uppermost layers of snow, firn, and ice, CO_2 values recorded in ice cores have been smoothed over intervals of decades. Law Dome ice was deposited rapidly, and the estimated smoothing interval is short enough (~20 years, Etheridge *et al*., 1996) to register even short-term changes in atmospheric CO_2. As a result, the Law Dome CO_2 values in Figure 3 are well suited for analyzing the effects of the Black Death and American pandemics on CO_2 and climate. The smoothing interval for the slowly deposited Taylor Dome ice is estimated at ~140 years (Indermuhle *et al*., 1999). This resolution should suffice for analyzing the slow-developing and long-lasting depopulation that occurred from 200 to 600.

2. Methods Used to Test the Depopulation-CO_2-Climate Link

This section describes methods and assumptions used to evaluate the hypothesis that changes in carbon emissions caused by depopulation affected CO_2 oscillations during the last two millennia (Ruddiman, 2003). This analysis requires two key links: (1) quantifying the amount of carbon sequestration on abandoned land produced by the major intervals of depopulation; and (2) translating this carbon sequestration into changes in atmospheric CO_2.

2.1. *Deforestation and Reforestation: Human 'Forest Footprints'*

Deforestation by humans occurred in two major phases that had different impacts on the environment. The first phase, here termed agricultural deforestation, was the clearing of old-growth forests to open land for croplands and pastures. This phase accounted for the largest part of forest removal (Williams, 2003). In addition to making new land available to grow food, habitat of dangerous mammalian predators was reduced. Because the negative environmental impacts of this kind of clearance were relatively small and not much noted at the time, this early phase of deforestation received little comment from contemporary observers, particularly because much of it preceded the advent of written records. This phase of deforestation was featured in the hypothesis of Ruddiman (2003) and is the focus of this paper.

The second phase of deforestation, here referred to as resource deforestation, pertains to forested areas that remained on higher steeper terrain when most arable land had been cleared. Wood taken from these regions was used for building homes and ships, for cooking and heating, and for smelting of iron as societies advance in technological sophistication. Each of these uses of wood was roughly an order of magnitude smaller than the earlier losses to agricultural clearance (Williams, 2003). In many cases, the remaining forests became managed woodlots that were cyclically harvested.

This later phase of resource deforestation was widely noticed by contemporary observers, in part because the impending loss of the residual forests seemed threatening, and in part because of highly visible environmental damage (Bechmann, 1990; Elvin, 1993). Without forest cover, rainwater tended to run off steep slopes rather than being absorbed into the soil and water table. Hillsides eroded, rivers carried mud-laden runoff, and natural springs disappeared because of reduced ground-water flow. These two phases of deforestation overlap to some extent. Even in the early phases of agricultural deforestation, some timber was used for home building and some wood was burned for heating and cooking. But clearance of arable land was the predominant form of deforestation.

History provides a vital 'data point' for the analysis that follows. In 1086, William the Conqueror ordered a survey of his newly won land (England) that by chance gives a snapshot of an iron-age country very near the transition between the two phases of deforestation. The survey results, reported in 1089 in the Domesday Book, counted 1.5 million citi-

zens and determined that 90% of the arable land was in pasture or croplands. A meticulous analysis by Rackam (1980) based on wide-ranging historical and ecological methods confirmed both the pattern and extent of deforestation indicated by the Domesday survey. Perhaps as a result of the Domesday survey, William's heirs enacted laws restricting the access of commoners to the remaining forests.

The Domesday Book provides a basis for two kinds of quantitative estimates used in this study. The Domesday census and land-use numbers indicate that a population density of ~11 persons/km^2 was sufficient to deforest 90% of the arable land in England in the 11th century. With this value in hand, we can use historical population data from McEvedy and Jones (1978) and compilations of the amount of arable land (lying at <1km elevation) to estimate the time at which other regions inhabited by iron-age people reached a population density of 11/km^2 and thus (arguably) the point of full deforestation of arable land. Such an assumption is of course, crude, but in many regions it can be evaluated against historical and ecological sources.

Table 2 shows the estimated time when heavily populated regions of Europe and Asia would have reached the Domesday population threshold. In Europe, numerous sources suggest that most arable land in the Greco-Roman centers of early Mediterranean civilization was deforested by the start of the historical era (Hughes, 1975; Thirgood, 1981; Simmons, 1996; Roberts, 1998; Williams, 2003), in agreement with the estimates in table 2. Part of the expansion of the early Roman Empire entailed a search for timber to build ships and maintain dominance in the Mediterranean Sea.

Table 2 indicates that much of Western Europe reached the Domesday threshold between 1000 and 1300, an interval of rapid population growth. These estimates are consistent with data on forest losses in France and Germany between 1100 and 1350 (Bechmann, 1990) and with laws enacted to protect forest preserves in those regions during the 1200s and 1300s (Williams, 2003). In contrast, Scandinavia and countries in the easternmost Baltic were never fully deforested during medieval centuries. Exploitation of timber resources in those regions only occurred in the early modern period, when shipbuilding demands in Western Europe expanded.

We assume that the Domesday density threshold is also applicable to northern and central China where 'dry' farming of grain crops (primarily millet) and pasturing of livestock predominated, as in Europe. Chao (1986) reported that only a little more than 1 ha of land per capita was

tilled as of 2000 years ago but his estimates omitted pastures, hay fields, woodlots, dwelling areas, and (in some cases) fields left fallow between intervals of cultivation. In any case, the Yellow and Yangtze River valleys both passed the Domesday density threshold well before 2000 years ago, and historical ecologists have concluded that they were largely deforested at an early date (Hughes, 1975; Grigg, 1994; Simmons, 1996; Williams, 2003; Elvin, 2004). Historical evidence also suggests very early (pre-historical) deforestation of dry seasonal forest in grain-growing areas of the Indus River valley (Fairservis, 1971; Hughes, 1975).

It is unlikely that the Domesday density threshold can be applied to the rice-growing areas of southern China, the Ganges River area of northeastern India, and intervening lowland areas of southeastern Asia. In these regions, irrigation permitted very high food production per unit area, and people probably had a smaller per-capita impact on forested lands. Nevertheless, Chao (1986) reported that much of the deforestation of South China for agriculture was already confined to mountainous areas by the eighth to eleventh centuries, implying that lowland (rice-growing) regions were already fully occupied by rice farmers. The estimated date of 1100 for agricultural deforestation in this area (Table 2) agrees with this analysis (McNeill, 1997).

In any case, rice consumption favored such rapid population growth that population densities in such regions soon grew to several times the Domesday threshold. As a result, very early deforestation of the Ganges River valley of India and Bangladesh (prior to 2000 years ago) has been widely deduced by several studies (Fairservis, 1971; Hughes, 1975; Grigg, 1994; Simmons, 1996; Williams, 2003). Other regions in Southeast Asia (Japan, Indonesia, and Korea) appear to have passed the Domesday population density threshold by ~1000 or soon after (Table 2).

The Domesday density value of 11 people/km^2 is useful in a second way. Inverted, it yields an average per-capita 'forest footprint' for each iron-age human of 9 hectares (9 ha, or 0.09 km^2). Each human clears that much land, primarily for agriculture. This average per-capita value implicitly allows for the small fraction of England's population that was not engaged in farming and also for the fact that some members of farm families did not personally clear any land. We assume that Europeans living in iron-age cultures and in regions where the arable land had not yet been deforested occupied a farmland footprint of 0.09 km^2 prior to the onset of the late-Roman depopulation interval and the Black Death pandemic waves.

In contrast, the depopulation episode caused by the American pandemic between 1500 and 1750 killed people who were living in a late Neolithic ('stone-age') culture. The per-capita forest clearance for these people was lower than that for iron-age cultures.

Gregg (1988) estimated the amount of land needed by a typical Neolithic European village for crops, pastures, livestock, and fuel wood. She arrived at a per-capita estimate of 3 ha (0.03 km^2) of cleared land. Most of this amount represented pastures and hayfields. Woodlot needs were smaller, and croplands smaller still. The three-fold increase between this 3-ha estimate and the 9-ha Domesday value presumably reflects the intervening appearance of iron-age axes and plows, as well as the domestication of draft animals that dislodged stumps and pulled plows.

Estimates of the per-capita 'forest footprint' in the pre-Columbian Americas range between a few tenths of one ha to more than 2 ha (Maxwell, 1910; Heidenrich, 1971; Hurt, 1987; Williams, 2003). Values toward the lower end of this range tend to focus only on areas under 'current' cultivation for major crops and thus omit other factors: fields that lie fallow, frequent movements to new plots, and the use of forest wood for fuel.

Another reason this range is lower than the 3-ha value for Neolithic Europe is that most indigenous Americans kept no livestock and had no need of pastures and hay fields. But, presumably to fill their nutritional needs, they made wide use of fire to open and maintain clearings so that they could attract game and encourage growth of berries, nuts, and other foods. Although the extent of burning is difficult to estimate (Vale, 2002), it may have been one of the primary alterations of the landscape in pre-Columbian North America.

Plausible allowance for areas that were burned repeatedly (and thus kept 'deforested') would presumably bring the forest-footprint estimates for the Americas more in line with that from late Neolithic Europe. We assume here that every indigenous American occupied a forest footprint of 2 ha (0.02 km^2), half or less in croplands and woodlots, and the balance in areas burned repeatedly (and thus kept open). These forest-footprint estimates (9 ha for iron-age Europe and 2 ha for late Neolithic America) bracket estimates of 5-8 ha for primitive modern cultures living in conditions intermediate between a stone-age and iron age existence (Lawrence *et al*, 1998; personal communication, 2004).

To convert these 'forest footprint' estimates of early farmers to specific amounts (tons) of carbon, we need to know the average carbon density of specific types of forest in various regions. Houghton (1999) estimat-

ed the amount of carbon released by converting specific types of forest to pasture or cropland. The values ranged from less than 1000 tons per km^2 for dry forest to almost 3000 tons of carbon per km^2 for rain forest. We use Houghton's estimates to calculate the amount of carbon sequestered per unit area when cropland or pasture reverted to the type of forest natural to each area.

To estimate the total amount of carbon sequestered on abandoned farms, we calculate the product of the number of people killed during a pandemic interval, the average 'footprint' of farmland occupied per person, and the carbon content per unit area of land that reverts to forest:

Total carbon sequestered = (# people) x (km^2/person) x (tons carbon/km^2).

The very large amounts of carbon involved in these calculations are referred to as GtC, or billions of tons of carbon (1 Gigaton=1 Petagram=10^{15} g).

2.2. *Converting Changes in Atmospheric Carbon to Atmospheric CO_2 Anomalies*

The second major step in assessing the effects of major depopulation episodes is to transform estimates of the amount of carbon sequestered in reforestation into net changes in atmospheric CO_2 concentration. If all of the carbon sequestered by the vegetation were only exchanged with the atmosphere, the exchanges would occur in the ratio 2.13 GtC/1ppm CO_2, based on the weight of CO_2 in the atmosphere. For example, the preindustrial CO_2 concentration of 282 ppm is equivalent to 600 GtC (282 ppm x 2.13 GtC/ppm = 600 GtC).

In nature, however, exchanges of terrestrial carbon are not limited to the atmospheric reservoir. Rapid exchanges occur between the atmosphere, the surface ocean, and the vegetation and soil reservoirs over years to decades to centuries, while exchanges between these surface reservoirs and the deep ocean occur over centuries to millennia.

If a sudden decrease in terrestrial carbon emissions occurs, it will produce an abrupt drop in atmospheric CO_2, but within 50 years the signal in the atmosphere will have relaxed nearly half way back toward the preinput concentrations (Fig. 5; based on Fig. 1 of Joos *et al.*, 2004). The later phase of the relaxation is slower much because of the slow carbon exchanges with the deep ocean and the even slower exchanges between deep water and sea-floor $CaCO_3$. Even after several millennia, an estimated 10% of the initial carbon perturbation still remains in the atmosphere. In summary, the CO_2 concentration of the atmosphere at any 'current'

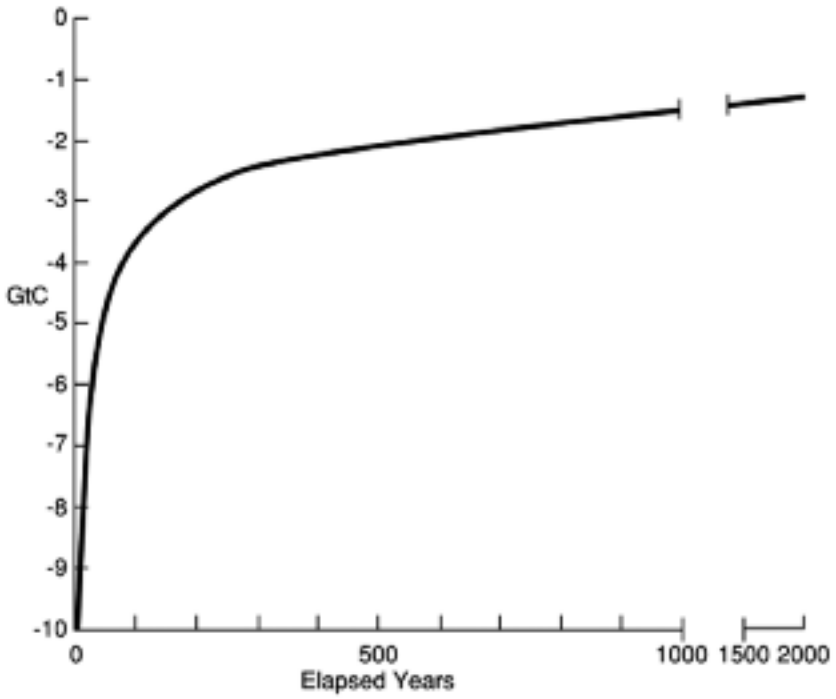

Figure 5. Impulse response based on Joos *et al*. (2004) showing the effect of carbon exchanges on the carbon content of the atmosphere. After sudden removal of 10 GtC, the atmospheric perturbation decreases rapidly for decades, then much more slowly for centuries and millennia.

time is significantly effected by carbon emissions in preceding decades, but it also retains a significant 'memory' of emissions from centuries ago.

To model the changes in atmospheric carbon and CO_2 concentrations that would occur in response to carbon sequestration during historical intervals of major depopulation, we use historical population data, human 'forest footprint' estimates, and carbon-density information to establish the time-varying pattern of carbon sequestration. Because most historical population data are available at no better than multi-decadal resolution, and because ice cores smooth changes in atmospheric CO_2 over similar intervals, we estimate changes in 50-year time steps.

We then move the impulse response function shown in Figure 5 across these time-varying estimates of carbon sequestration. The pertur-

bations caused by carbon sequestration after pandemics and other depopulation episodes die off in the same manner as the function in Figure 5: quickly at first and then much more slowly for centuries to millennia. This pattern simulates the operation of complex carbon-climate models by distributing carbon quickly among fast-reacting surface reservoirs and then more slowly with the deep-ocean and ocean-sediment reservoirs. The filter moves forward in time steps of 50 years, equivalent to the resolution of the historical depopulation estimates.

3. Modeling the Effect of Depopulation on Carbon Budgets

Three possible links exist between intervals of large-scale depopulation and decreases in atmospheric CO_2. As noted in sections 1 and 2, pandemics may have caused reforestation of abandoned farms, thus sequestering large amounts of carbon, and driving atmospheric CO_2 to lower values (Ruddiman, 2003). Here we use the approach outlined in the previous section to evaluate the effects of reforestation.

In addition, we evaluate the potential impact of two additional factors on atmospheric CO_2 concentrations – reduced rates of global-mean deforestation during and after the three major pandemics, and reduced rates of pre-industrial coal burning during the major depopulation of China in the 1200s and 1300s. Given the uncertainties involved in all of these analyses, the results presented are best regarded as a first-order test of the plausibility of these links, rather than as a definitive quantification of their size.

3.1. *Reforestation*

Ruddiman (2003) cited evidence from historians and historical ecologists for widespread abandonment of farms and farm villages during the two plague pandemics in Europe (McNeill, 1976; Rackam, 1980; Thirgood, 1981; Taylor, 1983). Reforestation is a foregone conclusion for the American pandemic, given the mortality rates of 85-90% (Denevan, 1992; Williams, 2003).

Evidence from land-use modeling (Houghton, 1999) indicates that forests will reclaim abandoned farmland in 50 to 100 years as dense stands of carbon-rich brush and saplings. Well within 100 years, the vegetation regains the equivalent carbon density of a mature forest. If successive waves of pandemic disease recur over a half-century or more,

large amounts of carbon will continue to be sequestered on land that had previously been devoted to agriculture.

Reforestation occurs only if no major population 'excess' exists to re-occupy the abandoned farms. If an excess does exist, farms are unlikely to revert to nature because other people soon resettle them. Based on the estimates in Table 1, we eliminate north-central China from this reforestation analysis, despite the large population drops shown in Figure 1a. The high population densities in northern and central China since before 2000 years ago should have provided a large excess of people to occupy abandoned land. Population densities in southeastern China were also high enough by 1000 years ago to leave it out of consideration.

For Europe during the late Roman Era and Black Death pandemics, we use estimates of pandemic mortality from McEvedy and Jones (1978), who subdivided population estimates for Europe along the boundaries of modern countries. We use the footprint of 9 ha (0.09 km^2) for European iron-age cultures. For the interval of depopulation spanning the late Roman era and subsequent centuries, we assume that each death led to per-capita farm abandonment in all of Europe except Greece and Italy, the only two regions that had already surpassed the Domesday population threshold (Table 2). For these regions, we assume no farm abandonment.

By the time of the Black Death, southwestern Europe had reached the Domesday threshold (Table 2). We assume that all farms in this region were re-occupied because population densities exceeded the threshold, but that none were re-occupied in northeastern Europe, Scandinavia and European Russia, where densities were low. Williams (2003) showed substantial reforestation of the northern plains of Germany after the Black Death.

For the American pandemic, Denevan (1992) subdivided pre-Columbian American populations at continental to subcontinental scales. We use the 2 ha (0.02 km^2) forest footprint for the American Neolithic cultures. In view of the 85-90% mortality rate for the American pandemic, we assume no reoccupation of abandoned regions, except for Aztec Mexico. In that region, the Spanish moved in quickly with their livestock, thus preventing major reforestation in lower-lying areas, but not in more heavily forested high terrain. We assume a reforestation rate of 75% for Mexico.

The product of the total mortality, the human 'footprint', and the forest-specific carbon sequestration yields estimates ranging from ~8 to ~14 Gt of carbon sequestration for the three pandemics (Table 3). These totals need to be allocated as time-varying amounts of sequestration across the duration of each pandemic.

McEvedy and Jones (1978) estimated that the population of Europe decreased nearly linearly between the geographically extensive Antonine 'plague' in 165-180 and the severe plague of Justinian in 540-542. Afterward, populations remained low for several centuries as lesser plague outbreaks continued. To approximate this continuous loss of population (and reforestation of abandoned land), we apportion the estimated 7.7 Gt of sequestered carbon from reforestation (Table 3) evenly across the interval 200 to 600 at a rate of 0.96 GtC per half century. We add a lag of 50 years to allow for the time required for abandoned farms to be covered by young forests.

The model simulation indicates that the atmosphere would have registered a maximum decrease of 2.2 GtC in the atmosphere by the interval 600-650 (Fig. 6a). Because the worst phase of this depopulation episode ended by 600, the major phase of reforestation should have come to an end by that time as well, even though plague outbreaks continued afterward. In the following centuries, carbon levels in the atmosphere slowly rose toward their prior concentration.

The severe Black Death outbreak from 1347 to 1353 was followed by smaller recurrences of plague over the next century. Of the total of 8.2 GtC estimated to have been sequestered during this pandemic (Table 3), we allocate 6 GtC to the interval 1350-1400 and the other 2.2 GtC to the interval 1400-1450. The model simulation (Fig. 6a) indicates that the atmosphere would have registered a maximum decrease of ~3.2 GtC between 1400 and 1450. For a brief interval between 1450 and 1500, following the Black Death but before the start of the American pandemic, the model simulates a brief rebound in atmospheric carbon (Fig. 6a).

Historical evidence suggests that the effects of European diseases were most devastating during the early phase of the American pandemic. Very high mortality is recorded by the 1520s and 1530s among the Aztecs, Incas, and populations in river valleys of southern North America (Denevan, 1992; Newson, 2001). We allocate the estimated 13.8 Gt of total carbon sequestration during the American pandemic as follows: 5 GtC in the half-centuries from 1550 to 1600 and from 1600 to 1650, and 1.9 GtC in the intervals from 1650 to 1700 and from 1700 to 1750. The model simulates a maximum decrease in atmospheric carbon of ~4.3 Gt from 1600 to 1650 (Fig. 6a). Much of this anomaly lingers into the 1700s and 1800s, by which time Europeans had begun to settle in the Americas in large numbers and deforest (or 're-deforest') many regions that had already been deforested prior to the pandemic.

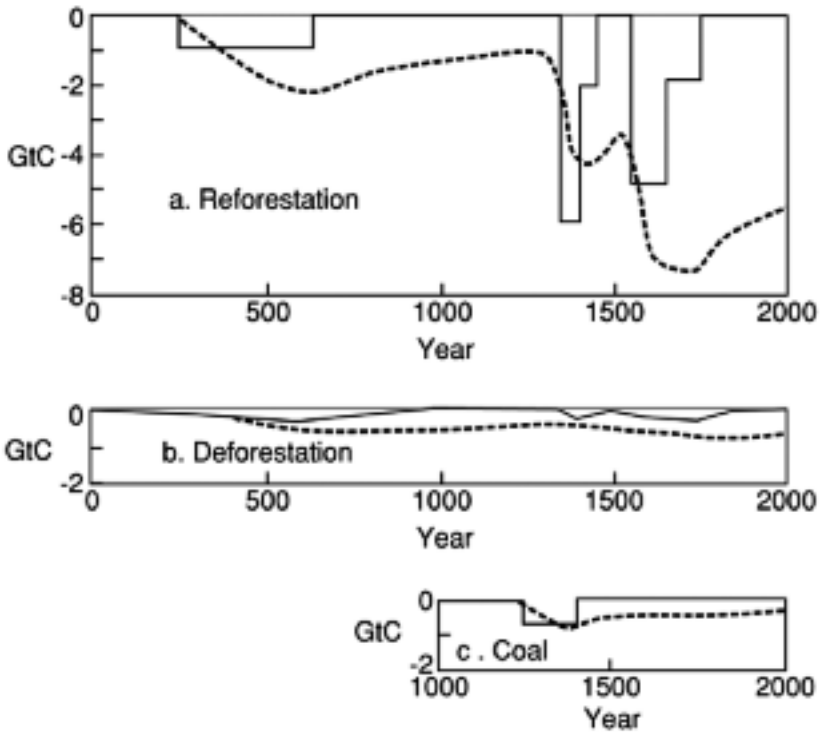

Figure 6. Model simulation of effects of major depopulation intervals on atmospheric carbon. Solid lines are estimated decreases in atmospheric carbon based on historical and ecological data. Dashed lines are model simulation of effects on the atmosphere after exchanges with other carbon reservoirs. Reforestation (A) has the largest effect on carbon reductions, with smaller effects from reduced deforestation (B) and coal burning (C).

3.2. *Reduced Deforestation*

In addition to causing reforestation, pandemics can also affect carbon budgets by reducing the rate of global deforestation. By killing a sizeable fraction of the humans that had previously been cutting forests, pandemics reduce the amount of carbon emitted to the atmosphere.

It is not possible to make region-by-region estimates of rates of deforestation during the historical era prior to industrial times. Such estimates would require detailed knowledge of growth rates of each regional population through time, yet population estimates for these times are inexact.

Calculating first derivatives (rates of change) of these already-uncertain numbers would greatly amplify the errors.

We can, however, make a very crude estimate of the reductions in deforestation rates by taking an indirect approach. First, we estimate the mean global rate of carbon emissions from deforestation across the last two millennia. For this, we use the estimate from Ruddiman (2005) that anthropogenic emissions prior to the industrial era amounted to a total of ~200 GtC. The rising CO_2 concentration in the atmosphere shown in Figure 3 can be used as a guide to partition this 200 GtC total across the last 8000 years. We assume that emissions began at 0 GtC/century 8000 years ago and rose to ~4 GtC/century by 2000 years ago. It then fluctuated around that value until the start of the industrial era. These estimates yield total emissions of just under 200 GtC for the pre-industrial era. The value of 4 GtC/century fits within estimates from Joos *et al*. (1999) of terrestrial carbon emissions (natural plus anthropogenic) during the last millennium.

Next we estimate the fractional reduction in global-mean carbon emissions caused by each pandemic. For simplicity, we assume that deforestation ceased entirely in pandemic-stricken regions because of pervasive mortality and related social disruption. We use Table 2 as a guide to eliminate regions that had previously reached the end of the agricultural phase of deforestation. In Table 4, we list the populations of all naturally forested regions that were still being actively cleared for agriculture at the time each pandemic struck. We calculate the size of the pandemic-stricken population as a percentage of this 'global' estimate. Finally, we allow for the fact that the first two (European) pandemics struck iron-age cultures, while the last (American) one ravaged a stone-age (Neolithic) culture. We assume that the rate of forest clearance in stone-age cultures was 22% of that in iron-age cultures, in proportion to the ratio of the iron-age and stone-age per-capita footprints (9 ha and 2 ha) and we adjust the calculations to incorporate this factor.

Using this method, we estimate fractional reductions in global carbon emissions at the peak of each pandemic: 13% for the late Roman era depopulation, 5% for the 14th century (Black Death) pandemic, and 14% for the American pandemic (Table 4). We then multiply the global-mean rate of carbon emission from deforestation (4 GtC/century) by the maximum fractional reduction in each pandemic to estimate the (maximum) net reduction in carbon emissions from deforestation. The values calculated are: ~0.5 GtC/century for the pandemic that began in the Roman Era, 0.2 GtC/century for the Black Death pandemic, and 0.6 GtC/century for the American pandemic.

We distribute these carbon-emissions reductions across the span of each pandemic interval in Figure 5b based on the mortality rates estimated by McEvedy and Jones (1978) and Denevan (1992). The effect of deforestation on carbon budgets differs from that of reforestation in two respects. First, the reductions in carbon emissions to the atmosphere are immediate, unlike the multi-decadal delay of carbon sequestration due to slow reforestation and carbon uptake after the pandemics. Second, the reduced rate of carbon emissions continues until the stricken population recovers. After the late Roman Era pandemic, European populations did not fully recover until 1000 (McEvedy and Jones, 1978). In contrast, recovery was well underway by 1500, only 150 years after the Black Death (Landers, 2004). In the case of the American pandemic, native populations had not even begun to recover by 1800 when Europeans arrived in large enough numbers.

In general, the simulated impact of reduced deforestation on the carbon budget of the atmosphere is considerably smaller than that from reforestation (Fig. 6b). Carbon reductions for all intervals in the last 2000 years are tenths of a GtC, compared to estimated values of several GtC for reforestation. Deforestation contributes a small amount to carbon reductions in the atmosphere during and after pandemics.

3.3. *Reduced Burning of Coal*

A third factor that could have affected pre-industrial atmospheric CO_2 concentrations is burning of coal in China. Because of early deforestation in northern and central China, coal was used as a source of fuel for heating and cooking long before the pre-industrial era. People extracted coal from surface outcrops and shallow pit mines using iron tools and then burned it in small braziers (hibachi-like stoves) in their homes. By the middle of the Song Dynasty (1040-1200), burning of coal was common in the north, while firewood was rationed and charcoal making forbidden. Hartwell (1962, 1967) estimated that all domestic fuel by the twelfth century was coal (apparently referring to northern China). Most of the documented coal use was domestic, although the Chinese may have begun using coal to produce iron.

China experienced substantial depopulation in the early centuries of the modern era, but the magnitude of these decreases is difficult to estimate because fluctuations in registered populations could simply reflect collapse of the census system. We restrict the focus of this section to the Mongol era from 1279 to 1368 (Figure 1b). Estimated population losses

are very high because the Mongols destroyed much of the economic infrastructure and also implemented genocidal policies (Deng, 2003). Recovery began with the Ming dynasty after 1400.

For this analysis, we assume a net mortality of 40 million people in China between 1200 and 1400 (Table 1). A simple but crude calculation can be made of the maximum possible impact of this level of mortality in reducing carbon emissions from coal burning. We assume that each 5-person family that used coal burned a total of 10 kg per day, of which 50% by weight was carbon. Each family would have emitted ~5 kg of carbon/day, or 1.8 tons/year. If the 40 million deaths occurred in ~8 million families that burned coal, the total reduction in carbon emissions would have been ~14.4 million tons/year. Over the course of the 150 years between 1250 and 1400, the total reduction in emissions would have been ~2.2 GtC. We allocate this 2 GtC as reductions of 0.73 GtC for each 50-year interval between 1250 and 1400.

We use the filter in Figure 5 to estimate the effect of this reduction in carbon emissions on the amount of carbon in the atmosphere. The maximum simulated lowering from reduced burning of coal is 0.83 GtC from 1350-1400 (Fig. 6c).

4. The Effects of Depopulation on Atmospheric CO_2

The simulated reductions in the carbon content of the atmosphere (Fig. 6) can be directly converted into estimates of the reductions in atmospheric CO_2 (Fig. 7, see page 411). As noted in section 2, this conversion follows the pre-industrial atmospheric ratio of 2.13 (the change in GtC per 1 ppm change in CO_2). In effect, we simply scale the GtC changes in Figure 6 to this ratio in order to plot Figure 7. In this section, we evaluate the separate (and then combined) effects of reforestation, reduced deforestation, and reduced coal burning on atmospheric CO_2. Estimated changes in atmospheric CO_2 are plotted at the same scale as the CO_2 'target signal' (Fig. 7a).

Reforestation. The CO_2 anomaly that developed during the depopulation interval spanning the late Roman era reached a maximum simulated value of ~1 ppm by 600-650 (Fig. 7b). The gradual development of this anomaly resembles the (poorly-dated) CO_2 anomaly measured at Taylor Dome (Figs. 2b, 7a), and the simulated anomaly accounts for about half of the amplitude of the measured CO_2 anomaly. For the Black Death, the model simulates a short-lived CO_2 drop of ~1.5 ppm between 1400 and 1450. This value represents more than half of the (noisy) CO_2 decrease of ~2 ppm recorded in the

well-dated Law Dome record. For the American pandemic era, the model simulates a CO_2 decrease of just over 2 ppm between 1650 and 1700 (Fig. 7b). This CO_2 drop represents about 40% of the ~5 ppm CO_2 decrease observed between 1500 and 1750 at Law Dome. In all three cases, carbon sequestration caused by reforestation provides a plausible explanation for roughly half (or more) of the CO_2 decreases measured in the ice cores.

Deforestation. Deforestation has only a second-order impact on atmospheric CO_2 values during pandemics (Fig. 7c), although the relative impact of the long-lasting depopulation episodes that followed the late Roman era and American pandemics are not negligible. Together, reforestation and reduced deforestation appear to account for half of the observed CO_2 drops during the three pandemic episodes.

Coal Burning. The reduction in burning of coal from shallow pit mines caused by ~40 million deaths in China between 1250 and 1400 causes an estimated CO_2 drop of ~0.4 ppm between 1350-1400 (Fig. 7d). Like reduced deforestation, reduced coal burning is a second-order factor in past changes in atmospheric CO_2.

4.1. *Combined Effects of Depopulation Episodes on Atmospheric CO_2*

Atmospheric CO_2 concentrations rose at a relatively steady rate from 8000 to 2000 years ago, but then leveled off and began to oscillate erratically (Fig. 3). Ruddiman (2003) proposed that the reason for both the change in trend near 2000 years ago and the subsequent oscillations might be linked to the effects of major pandemics in sequestering carbon and reducing the amount of carbon in the atmosphere.

The model-simulated effects of reforestation, reduced deforestation and reduced coal burning are combined in Figure 8b (see page 412). The short-term effects of the major depopulation episodes – the CO_2 decreases at and after 200, 1350, and 1500 – are the most obvious feature of this trend. But the atmosphere has a long 'memory' for carbon emissions in prior centuries and even prior millennia, and substantial effects of these episodes linger for centuries and millennia afterward.

This trend can be compared against the CO_2 'target signal' shown in Fig. 8a. The plot in Figure 8b does not attempt to simulate the (unknown) changes in agricultural deforestation that were underway in many regions of the world through the last two millennia. Increases in deforestation would have driven atmospheric CO_2 concentrations to higher values. Instead, this plot summarizes only the extent to which depopulation

episodes could have slowed the long-term increase in atmospheric CO_2 that had been underway for millennia (Fig. 3)

The ~1 ppm CO_2 reduction that occurred during the late Roman era had decreased to about 0.7 ppm just before the effects of reduced coal burning in China and the Black Death pandemic began to be felt. An abrupt increase in Eurasian populations between 1000 and 1300 (McEvedy and Jones, 1978) may have caused increased deforestation and driven CO_2 values sharply higher at that time (Fig. 8b).

Subsequently, three depopulation episodes occurred within a relatively short time. The combined effects of reduced coal burning in China, the Black Death pandemic in Eurasia, and the American pandemic drove CO_2 concentrations ~4 ppm lower than the values reached in 1100-1200. This drop represents just over half of the 7-8 ppm decrease in ice-core CO_2 measured between 1100 and 1700 (Fig. 8a). It appears that depopulation (mainly through pandemics) imposed a net CO_2 decrease of ~4 ppm on the rising trend that had been underway for many millennia (Fig. 3). This analysis does not take into account the possible role of climate-system feedbacks in amplifying CO_2 changes imposed by depopulation episodes.

The net simulated decrease of ~4 ppm that might be explained by pandemics and other causes of depopulation between 1000-1200 and 1500-1750 would result in a net global cooling of about 0.05°C. This estimate represents about one third of the century-scale cooling between 1000-1200 and 1500-1750 estimated by Mann *et al.*, (1998) and Crowley and Lowery (2000). A vigorous debate is underway as to whether these temperature estimates for the last millennium are valid or whether the actual cooling was larger. Within this ongoing uncertainty, pandemic-driven effects on reforestation and carbon sequestration could range from a significant factor in a small cooling to a secondary factor in a larger cooling.

An interesting sideline of this analysis is the fact that the simulated (and lingering) effects of these historical pandemic intervals make the CO_2 concentration in the modern atmosphere ~3 ppm lower than it would be in their absence (Fig. 8b).

5. Discussion and Conclusions

Variations in population (Fig. 1) and climate (Fig. 2) appear to have been coupled during the historical era. Invoking a form of environmental determinism, Lamb (1977) proposed a causal chain in which cooler cli-

mates reduced food production, causing famine and death as direct results, and also produced malnutrition and disease that led indirectly to additional mortality. Historical demographers have criticized this hypothesis on the basis that mortality from even the largest pre-industrial famines was neither large enough nor persistent enough to have a first-order effect on populations (Watkins and Menken, 1985, 1988). Climate scientists have voiced doubts that the changes in temperature proposed by Lamb would have had significant effects on food production, as they would have had impacts only in colder regions at high latitudes and altitudes that are at best marginally suitable for agriculture, and thus not heavily occupied by humans (Le Roy Ladurie, 1971; Pfister *et al*., 1999). The small size of the temperature changes reconstructed for the northern hemisphere (Figure 2a) adds weight to this criticism.

Nevertheless, large-scale depopulation episodes during the historical era do appear to correlate with drops in atmospheric CO_2 levels and decreases in northern hemisphere temperature (Figs. 1, 2). Given the inability of volcanic eruptions and changes in solar irradiance to account for CO_2 drops as large as 8 ppm without violating hemispheric and global temperature constraints, pandemics and depopulation episodes are a potential casual link.

Three plausible mechanisms could link major historical depopulation episodes with CO_2 decreases and climate: reforestation of abandoned lands, reduced rates of deforestation, and reduced burning of coal. Our analysis suggests that reforestation was the primary mechanism that lowered CO_2 concentrations, that reduced rates of deforestation played a lesser role, and that reduced coal burning was also relatively unimportant. Given the large number of assumptions required for these analyses, the results summarized here should be viewed as a demonstration of the feasibility (plausibility) of these links, but not as a demonstration of proof.

If our basic conclusions are correct, disease and climate are linked historically, but in an indirect way. Rather than changes in climate causing changes in population (as in Lamb, 1977), both climate and population respond to an independent driver – the massive level of mortality during pandemics and other major depopulation episodes.

APPENDIX

TABLE 1. Population estimates for China (in millions).

Age	McEvedy and Jones (1978)	Biraben (1979) and Livi-Bacci (2001)
200 BCE	40	40
1 CE	50	70
200	60	60
400	50	25
600	45	49
800	50	56
1000	60	56
1100	100	83
1200	115	124
1300	85	83
1400	75	70
1500	100	84
1600	150	110
1650	130	100-150
1700	150	190-225
1750	215	220
1800	320	320-330

TABLE 2. Estimated dates when populations for various regions* would have reached the Domesday density threshold of 11 persons/km^2.

Continent/ Country/ Region	Domesday Population Threshold (10^6 People)	Date Threshold Reached
Asia		
N. China, Yellow River	9	before 0
C. China, Yangtze River	9	before 0
NE India, Ganges River	12	before 0
NW India, Indus River basin	8	before 0
Japan	0.7	300
South-Central India	1.7	700
Indonesia	3.3	800
Southern China	4	1100
Korea	2.2	1100
Europe		
Greece	0.6	before 0
Italy	1.7	before 0
Czechoslovakia	1.1	800
France	6.1	1000
Belgium/Netherlands	0.7	1000
Austria	0.6	1000
British Isles	2.5	1100
Spain/Portugal	5.3	1100 (200)
Germany	5.2	1200
Hungary	1.0	1300
Poland	3.4	1300

* McEvedy and Jones (1978), Denevan (1992).

TABLE 3. Estimated sequestration of carbon (in Gt = 10^9 tons) by reforestation of farmland (crops and pastures) abandoned because of high pandemic mortality.

Pandemic (region)	Forest type	Mortality** (millions)	Per-capita Footprint (km^2)	C Sequestered (Tons/km^2)	GtC Sequestered
Late Roman Era (200-800)					
Scandinavia	Conifer	-0.1	0.09	1350	-0.1
N-C Europe	Deciduous	3.05	0.09	1630	4.5
S Europe	Mediterranean	2.05	0.09	1820	3.3
				Total	~7.7
Black Death (1350-1450)					
Scandinavia	Conifer	0.5	0.09	1350	0.6
N-C Europe	Deciduous	2.6	0.09	1630	7.6
				Total	~8.2
American (1500-1750)					
N. America	Deciduous	3.5	0.02	1630	1.1
Mexico	Seasonal/dry	15	0.02	800	2.4
Amazon	Tropical Wet	15	0.02	2190	6.6
Andes	Montaine	14	0.02	1300	3.7
				Total	~13.8

** Mortality shown only for regions still in process of being deforested (Table 1).

TABLE 4. Rates of deforestation in pandemic-stricken areas as a fraction of all regions still undergoing deforestation on a global basis.

200-800 Epidemics and Pandemic			
Region	Population Deforesting (m)	Correction for stone tools	Adjusted Rate of Deforestation
Pandemic: Europe	*5.2*	-	*5*
Other:			
Asia	25	-	25
Africa (Sub-Sahara)	5	x 0.22	1
Americas	30	x 0.22	7
Global Total			38
Pandemic deforestation as a fraction of the global total: 5/38 = ~13%			

1350-1450 Pandemic			
Region	Population Deforesting (m)	Correction for stone tools	Adjusted Rate of Deforestation
Pandemic: Europe	*3.1*	-	*3*
Other:			
Asia	36	-	36
Africa (Sub-Sahara)	22	x 0.22	5
Americas	49	x 0.22	11
Global Total			55
Pandemic deforestation as a fraction of the global total: 3/55 = ~5%			

1500-1750 Pandemic			
Region	Population Deforesting (m)	Correction for stone tools	Adjusted Rate of Deforestation
Pandemic: Americas	*48*	*x 0.22*	*11*
Other:			
N. Europe	15	-	15
Asia	46	-	46
Afica (Sub-Sahara)	31	x 0.22	7
Total			79
Pandemic deforestation as a fraction of the global total: 11/79 = ~14%			

REFERENCES

Barnola, J.M., Anklin, M., Procheron, J., Raynaud, D., Schwander, J., and Stauffer, B. (1995), CO_2 evolution during the last millennium as recorded by Antarctic and Greenland ice, *Tellus B* 47, 264-272.

Bechmann, R. (1990), *Trees and Man: The Forest in the Middle Ages* [1984], translated from the French by Katharyn Dunham, New York: Paragon House.

Biraben, J.N. (1979), Essai sur l'évolution du nombre des hommes, *Population* 34: 13-24.

Bourdelais, P. (2003), *Les Épidémies terrassées: une histoire de pays riches*, Dijon Quetigny: Éditions de La Martinière.

Carcallet, C., *et al*. (2002), Holocene biomass burning and global dynamics of the carbon cycle, *Chemosphere* 49, 845-863.

Chao, K. (1986), *Man and Land in Chinese History*, Stanford: Stanford University Press.

Chang (2002), Disease and its impact on politics, diplomacy, and the military: the case of smallpox and the Manchus (1613-1795), *Journal of the History of Medicine and Allied Sciences* 57, 177-197.

Crowley, T.J. (2000), Causes of climate change over the past 1000 years, *Science* 289, 270-277.

Crowley, T.J. and Lowery, T.S. (2000), How warm was the Medieval Warm Period? A comment on man-made versus natural climate change, *Ambio* 39, 51-54.

Denevan, W.M. (ed.) (1992), *The Native Population of the Americas in 1492*, 2nd ed., Madison: University of Wisconsin Press.

Deng, K.G. (2003), China: Tang, Song and Yuan Dynasties, *The Oxford Encyclopedia of Economic History*, J. Mokyr (ed.), 5 volumes (New York and Oxford: Oxford University Press) 2, 423-28.

Duncan-Jones, R. (1996), The Impact of the Antonine Plague, *Journal of Roman Archaeology* 9, 108-136.

Dunstan, H. (1975), The late Ming epidemics: a preliminary survey, *Ch'ing-Shih wen-t'i* 3, 1-59.

Eckert, E. (1996), *The Structure of Plagues and Pestilences in Early Modern Europe: Central Europe, 1560-1640*, New York and Basel: Karger.

Elvin, M. (1993), Three thousand years of unsustainable growth: China's environment from archaic times to the present, *East Asian History* 6, 7-46.

Elvin, M. (2004), *The Retreat of the Elephants: an Environmental History of China*, New Haven: Yale University Press.

Esper, J., Cook, E.R., and Schweingruber, F.H. (2002), Low-frequency signals in long tree-line chronologies for reconstructing past temperature variability, *Science* 295, 2250-2253.

Etheridge, D.M., Steele, L.P., Langenfields, R.L., Francey, R.J., Barnola, J.-M., and Morgan, V.I. (1996), Natural and anthropogenic changes in atmospheric CO_2 over the last 1000 years from air in Antarctic ice and firn, *Journal of Geophysical Research* 101, 4115-4128.

Fairservis, W.A., Jr. (1971), *The Roots of Ancient India*, New York: Macmillan.

Gerber, S., Joos, F., Brugger, P., Stocker, T.F., Mann, M.E., Sitch, S., and Scholze, M. (2003), Constraining temperature variations over the last millennium by comparing simulated and observed atmospheric CO_2, *Clim. Dyn.* 20, 281.

Gregg, S.A. (1988), *Foragers and Farmers: Population Interaction and Agricultural Expansion in Prehistoric Europe*, Chicago: University of Chicago Press.

Grigg, D.B. (1994), *The Agricultural Systems of the World*, Cambridge: Cambridge University Press.

Gutmann, M. (1980), *War and Rural Life in the Early Modern Low Countries*, Princeton: Princeton University Press.

Hartwell, R. (1962), A revolution in the Chinese Iron and Coal Industries during the Northern Sung, 960-1126 AD, *Journal of Asian Studies* 21, 153-162.

Hartwell, R. (1967), A cycle of economic change in imperial China: coal and iron in northeast China, 750-1350, *Journal of the Economic and Social History of the Orient*, 10, 102-159.

Hatcher, J. (1977), *Plague, Population and the English Economy, 1348-1530*, London: Macmillan.

Hatcher, J. (1994), England in the aftermath of the Black Death, *Past and Present* 144, 3-35.

Heidenrich, C. (1971), *Huronia: A history and geography of the Huron, Indians, 1600-1650*, Ontario: McClelland and Stewart.

Houghton, R.A. (1999), The annual net flux of carbon to the atmosphere from changes in land use 1850-1990, *Tellus B* 51, 298-313.

Hughes, J.D. (1975), *Ecology in Ancient Civilizations*, Albuquerque: Univ. New Mexico Press.

Hurt, R.D. (1987), *Indian Agriculture in America*, Kansas: Lawrence University Press.

Indermuhle, A., Stocker, T.F., Joos, F., Fischer, H., Smith, H. J., Wahlen, M., Deck. B., Mastroianni, D., Blunier, T., Meyer, R., Stauffer, B. (1999), Holocene carbon-cycle dynamics based on CO_2 trapped in ice at Taylor Dome, Antarctica, *Nature* 398, 121-126.

IPCC (2001), *Third Assessment Report of the Intergovernmental Panel on Climate Change*, Cambridge: Cambridge Univ. Press.

Jones, P.D., and Mann, M.E. (2004), Climate over Past Millennia, *Reviews of Geophysics* 42, 2003RG000143.

Jones, P.D., Osbourn, T.J., and Briffa, K.R. (2001), The evolution of climate over the last millennium, *Science* 292, 662-667.

Joos, F., Meyer, R., Bruno, M., Leuenberger, M. (1999), The variability in the carbon sinks as reconstructed for the last 1000 years, *Geophysical Research Letters* 26, 1437-1440.

Joos, F., Gerber, S., Prentice, I.C., Otto-Bleisner, B.L., Valdes, P. (2004), Transient simulations of Holocene atmospheric carbon dioxide and terrestrial carbon since the last glacial maximum, *Global Biogeochemical Cycles*, 18, GB2002 10.1029/2003GB002156.

Jordan, W.C. (1996), *The Great Famine: Northern Europe in the Early Fourteenth Century*, Princeton: Princeton University Press.

Lamb, H.H. (1977), *Climate: Past Present and Future*, vol. 2, London: Methuen.

Landers, J. (2004), *The Field and the Forge: population, production and power in the pre-industrial West*, New York and Oxford: Oxford University Press.

Lavely, W. and Wong, R.B. (1998), Revising the Malthusian narrative: the comparative study of population dynamics in late imperial China, *Journal of Asian Studies* 57, 714-748.

Lawrence, D., Peart, D.R., and Leighton, M. (1998), The impact of shifting cultivation on a rainforest landscape in West Kalimantan: spatial and temporal dynamics, *Landscape Ecology* 13, 135-148.

Lee, J.Z, and Feng, W. (1999), *One Quarter of Humanity: Malthusian Mythology and Chinese Realities, 1700-2000*, Cambridge, MA: Harvard University Press.

Le Roy Ladurie, E. (1971), *Times of Feast, Times of Famine: A History of Climate Since the Year 1000*, translated by Barbara Bray, Garden City, N.Y.: Doubleday.

Livi-Bacci, M. (2001), *A Concise History of World Population*, 3rd edition, Oxford: Blackwell.

Mann, M.E. and Jones, P.D. (2003), Global surface temperatures over the past two millennia, *Geophysical Research Letters* 30, doi: 10.10129/2003GL017814.

Mann, M.E., Bradley, R.S., and Hughes, M.K. (1999), Northern hemisphere temperatures during the past millennium: Inferences, uncertainties, and limitations, *Geophysical Research Letters* 26, 759-762.

Marks, R.B. (1998), It never used to snow: climatic variability and harvest yields in late-imperial south China, 1650-1850, pp. 411-446. In: *Sediments of Time: Environment and Society in Chinese History*, Mark Elvin and Liu Ts'ui-jung (eds.), Cambridge and New York: Cambridge University Press.

Maxwell, H. (1910), The use and abuse of the forests by the Virginia Indians, *William and Mary College Quarterly* 19, 73-104.

McEvedy, C., Jones, R. (1978), *Atlas of World Population History*, New York: Penguin.

McNeill, J.R. (1997), China's Environmental History in World Perspective, pp. 31-49. In: Mark Elvin and Liu Ts'ui-Jung (eds.), *Sediments of Time: Environment and Society in Chinese History*, New York: Cambridge University Press.

McNeill, W.H. (1976), *Plagues and Peoples*, New York: Doubleday.

Moberg, A., Sonechkin, D.M., Holmgren, K., Datsenke, N.M., Karlen, W. (2005), Highly variable Northern hemisphere temperatures reconstructed from low- and high-resolution proxy data, *Nature* 455, 613-627.

Newson, L. (2001), Pathogens, places and peoples: geographical variations in the impact of disease in early Spanish America and the Philippines, pp. 167-210. In: Raudzens, G. (ed.), *Technology, Disease and Colonial Conquests, Sixteenth to Eighteenth Centuries*, v. 2 of the Loyola College History of Warfare, Leiden: Brill.

Ó Gráda, C. (2005), Markets and famines in pre-industrial Europe, *Journal of Interdisciplinary History* 36, 143-166.

Overpeck, J.S., *et al*. (1997), Arctic environmental change of the last four centuries, *Science* 278, 1251-1256.

Paine, R.R. (2000), If a population crashes in prehistory and there is no paleodemographer there to hear it, does it make a sound?, *American Journal of Physical Anthropology* 112, 181-190.

Palmer, A.S., van Ommen, T.D., Curran, M.A.J., Morgan, V., Souney, J.M., and Mayewski, P.A. (2001), High-precision dating of volcanic events (A.D. 1301-1995) using ice cores from Antarctica, *Jour. Geophys. Res.* 106, 28, 089-28, 095.

Pfister, C., Brázdil, R., and Glaser, R. (eds.) (1999), Climatic Variability in Sixteenth-Century Europe and its Social Dimension, *Special issue of Climatic Change* 43, (1).

Rackam, O. (1980), *Ancient Woodland: Its History, Vegetation, and Uses in England*, London: Edward Arnold.

Richards, J.F. (1997), Early Modern India and World History, *Journal of World History* 8, 197-209.

Richards, J.F. (2003), *The Unending Frontier: An Environmental History of the Early Modern World*, Berkeley and Los Angeles: University of California Press.

Roberts, N. (1998), *The Holocene*, Oxford: Blackwell.

Ruddiman, W.F. (2003), The anthropogenic greenhouse era began thousands of years ago, *Climatic Change* 61, 261-293.

Ruddiman, W.F. (2005), Cold climate during the closest analog to modern interglaciation, *Quaternary Science Reviews* 24, 1121-1132.

Sallares, R. (2002), *Malaria and Rome: A history of malaria in Ancient Italy*, Oxford: Oxford University Press.

Sarris, P. (2002), The Justinianic plague: origins and effects, *Continuity and Change 17*, 169-182.

Scheidel, W. (2001), *Death on the Nile: Disease and demography of Ancient Egypt*, Leiden: Brill.

Shuie, C.H. (2005), The political economy of famine relief in China, 1740-1820, *Journal of Interdisciplinary History* 36, 33-56.

Siegenthaler, U., Monnin, E., Kawamura, K., Spahni, R., Schwander, J., Stauffer, B., Stocker, T.F., Barnola, J.-M., and Fischer, H. (2005), Supporting evidence from the EPICA Dronning Maud Land ice core for atmospheric CO_2 changes during the past millennium, *Tellus 57B*, 51-57

Simmons, I.G. (1996), *Changing the Face of the Earth*, Oxford: Blackwell.

Stathakopoulos, D.C. (2004), *Famine and Pestilence in the late Roman and Early Byzantine Empire: a systematic survey of subsistence crises and epidemics*, London: Ashgate.

Taylor, C. (1983), *Village and Farmstead*, London: George Phillip.

Thirgood, J.V. (1981), *Man and the Mediterranean Forest*, London: Academic Press.

Twitchett, D. (1979), Population and pestilence in T'ang China, pp. 35-68. In: Wolfgang Baue (ed.), *Studia Sino-Mongolica: Festschrift für Herbert Franke*, Wiesbaden: Franz Steiner Verlag.

Vale, T.R. (ed.) (2002), *Fire, Native Peoples, and the Natural Landscape*, Island Press: Washington, D.C.

Watkins, S.C., and Menken, J. (1985), Famines in historical perspective, *Population and Development Review* 11, 647-675.

Watkins, S.C., and Menken, J. (1988), On the role of crises in historical perspective, *Population and Development Review* 14, 165-170.

Williams, M. (2003), *Deforesting the Earth*, Chicago: Univ. Chicago Press.